Study of Nano structured SnO_2 doped MnO_2 Based LPG Sensors

R. R. Attarde[1], D. R. Patil[2]

[1]Department of physics, M. J. College, Jalgaon (MS) India

[2]Bulk and Nanomaterials Research Lab, Dept. of Physics, R. L. College, Parola (MS), India.

Abstract

The nano scaled material powder of MnO_2 was synthesized by Disc type ultrasonicated microwave assisted centrifuge technique. The characterizations and LPG gas sensing performance of pure and SnO_2 doped MnO_2 thick films have been investigated. Thick films of pure manganese oxide were prepared by screen printing technique. Pure manganese oxide was almost insensitive to LPG. However, SnO_2 doped MnO_2 (5 wt. %.) thick films were observed to be most sensitive to LPG (200 ppm) at 350^0C. The efforts are made to develop the LPG gas sensor based on doping of pure MnO2 thick films. The quick response and fast recovery are the main features of this sensor. The effects of microstructure and additive concentration on the gas response, selectivity, response time and recovery time of the sensor in the presence of LPG gas were studied and discussed.

Keywords: SnO_2 doped MnO2, LPG gas sensor, Thick film, Low cost sensor.

1. Introduction

It has been known for a long time that the adsorption of gas molecules on a metal oxide semiconductor surface can cause a significant change in the electrical conductivity of the material [1]. Their surface properties are sensitive to changes in the gaseous atmosphere, especially on small amounts of hydrocarbons and hydrogen [2]. Gas sensing in semiconductors like SnO_2 is achieved by the change in conductivity as a function of operating temperature, gas concentration, doping elements, doping concentrations, sintering parameters like temperature, period, etc. SnO_2 is an n-type semiconducting material in the field of gas sensors [3]. The gas sensing mechanism depends on chemical and electronic properties and on the three dimensional ordering of both the bulk and the surface which is affected by surface region of the grains / particles. Gopel et. al. emphasized that the development and improvement of a chemical sensor requires a balance between empirical knowledge and systematic research as long as the basic processes involved are unknown [4]. Accordingly, studying the structure as well as the volume and surface chemical composition, is of great importance to better understanding of gas sensing mechanism [5]. It is described as a chemical adsorption / desorption process of oxygen on the surface of sensing materials [6, 7], followed by a charge transfer mechanism between the adsorbate and surface of the sensing material, leading to a measurable change in the electrical resistance. During this mechanism a very thin space charge region is built at the surface leading to an increased electrical conductance. If the sensing material is exposed to a reducing environment, viz. atmosphere consisting CO, C_2H_5OH, H_2 or CH_4, surface reactions will result in a lower surface coverage of oxygen adsorbates and, therefore, in an increased conductance [8]. Oxidizing gases, such as ozone and nitrogen oxide, can also be detected by metal-oxide gas sensors [9, 10]. Regarding the chemical composition, it is of importance to know the stoichiometry because this affects the gas sensing properties of metal oxides [5]. The stoichiometry of tin oxide can lie between SnO and SnO_2. Additionally, different crystallographic phases of tin oxide exist. Generally, nonstoichiometric tin oxide (SnO_{2-x}) is used as sensors because oxygen vacancies are necessary for the gas sensing. Consequently, the chemical composition during synthesis needs to be optimized and a stable crystallographic structure and

stoichiometry must be formed for best sensor operations. In spite of many studies concerning the oxidation of SnO_x thin films prepared from SnO_2 precursors [11], only a little amount of work on the oxidation process of SnO nanoparticals was found in literature. Nevertheless, it is known that annealing treatments and structure influence the sensitivity of SnO_2 thin film gas sensors [12].

Over the past few decades, tin oxide based films are widely used as gas sensors due to their high sensitivity in the presence of trace amounts of some gases of interest viz. carbon monoxide, ethanol, methane, LPG, LNG, etc. Allied to this advantage is the low cost, simple, easier, robustness, fast response and recovery, selective nature to a particular gaseous species among the mixture of gases and the possibility of miniaturization of these devices [13 - 16]. The variation of the conductance measured under specific gases depends on many parameters such as intrinsic resistance, grain size [17], grain boundary barriers, detection temperature etc. Tin oxide films have been prepared by a number of techniques including spray pyrolysis [18, 19], sputtering [20, 21], chemical vapor deposition (CVD) [22] and evaporation [23].

The aim of the present work is to develop the low cost LPG sensors by utilizing the easily available material in large extent and modifying the material to enhance the LPG sensing performance. Pure and modified MnO_2 thick films are tested and developed, which could be able to detect the LPG at trace levels.

2. Experimental procedure

2.1 Synthesis of nanostructured powder

Nanostructured MnO_2 and SnO_2 doped MnO_2 powders were synthesized by disc type ultrasonicated microwave assisted centrifuge technique, by hydrolysis of AR grade manganese chloride in aqueous-alcohol solution. An initial aqueous alcohol solution was prepared from distilled water and propylene glycol in the ratio of 1:1. This solution was then mixed with aqueous solution of manganese chloride and tin chloride (dopant in the proportion 1, 3, 5 and 7 wt %) in the ratio such that the elemental concentration was 0.1M and the alcohol to water ratio was 1:1. The special arrangement was made to add drop wise aqueous ammonia (0.1ml / min.) with constant stirring until the optimal pH of solution becomes 8.6. After complete precipitation, the hydroxide was washed with distilled water until chloride ions were not detected by $AgNO_3$ solution. Then the hydroxide in a glass beaker was placed in a microwave oven for 10 minutes with on-off cycles, periodically. The dried precipitate was ground by agate pestle-mortar and annealed in a muffle furnace at 500°C for 3h. The phase purity and degree of crystallinity of MnO_2 powder were monitored by XRD analysis.

2.2 Thick Film Fabrication

The ultrafine powders of pure and SnO_2 doped MnO_2 were calcined at 500^0C for 3 h in air and reground to ensure sufficiently fine particle size. The thixotropic pastes were formulated by mixing the synthesized nanostructured powders of pure and doped MnO_2 (one at a time) with a solution of ethyl cellulose (a temporary binder) in a mixture of organic solvents such as butyl cellulose, butyl carbitol acetate and turpineol. The ratio of inorganic to organic part was kept as 80: 20 in formulating the pastes. The thixotropic pastes were screen printed on the glass substrates in desired patterns. Films prepared were dried at 80^oC under an IR lamp, followed by firing at 500^oC for 30 min in ambient air.

3. Material characterizations

3.1 Structural properties (X-ray diffraction studies)

X ray diffraction study of SnO_2 doped MnO_2 powders was carried out using BRUKER AXSD8 (Germany) advance model X ray diffraction with $CuK\alpha_1$ (λ=1.54056 Å) radiation in the 2θ range 20^0-80^0. The scanning speed of the specimen was maintained 0.5^0 /min. Fig. 1 shows the XRD pattern of SnO_2 doped MnO_2 powders. The 2θ peak observed at 26.19, 34.53, 37.62, 41.2, 42, 43.5, 45.32, 54.13, 61.04, 64.56, 71.3, 74 which correspond to the (200), (211), (220), (310), (220), (222), (321), (301), (112), (400), (510) and (420) planes of reflections. The XRD spectrum reveals that the materials are polycrystalline in nature and tetragonal in structure. The observed peaks are matching well with ASTM reported data of pure MnO_2. The material was observed to be nanocrystalline in nature. There are no prominent peaks of SnO_2 associated in XRD pattern of MnO_2 due to smaller wt % of SnO_2 in comparison with MnO_2. The lattice parameters were found to be a = 4.7365 and c = 3.2010. The unit cell volume was evaluated as 71.81. (JCPDS data card no. for Mn – 89 - 4836 and for Sn – 89 - 2761).

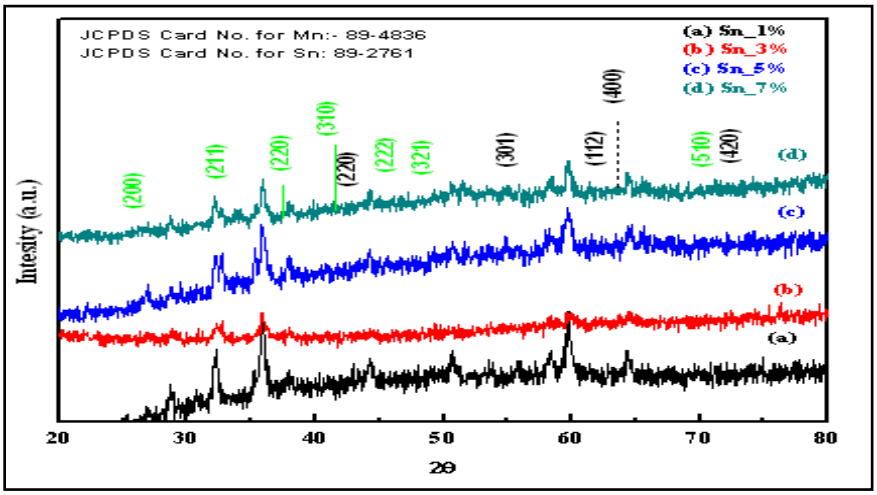

Fig. 1 XRD of SnO_2 doped MnO_2

3.2 Micro structural analysis (SEM)

3.2.1 Unmodified (Pure) MnO_2

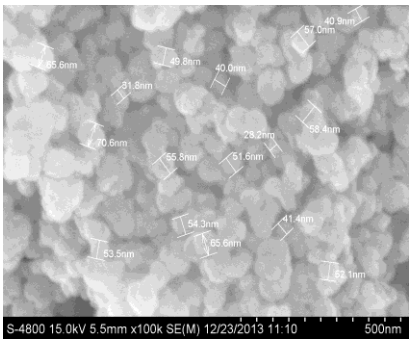

Fig. 2 **Micrograph of unmodified MnO_2 film**

Fig. 2 depicts the SEM image of pure MnO_2 thick film fired at 500^0C for 30 min. Pure MnO_2 thick film consists of voids and a wide range of randomly distributed grains with sizes ranging from 30 nm to 50 nm distributed as lumps.

3.2.2 SnO_2 doped MnO_2

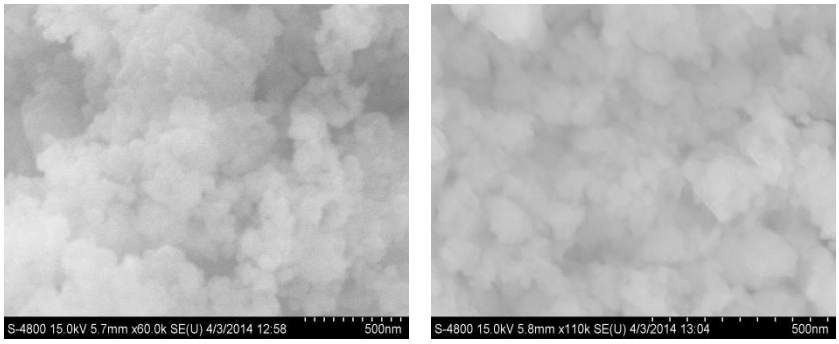

(a) 1 wt % SnO_2 doped MnO_2 (b) 3 wt % SnO_2 doped MnO_2

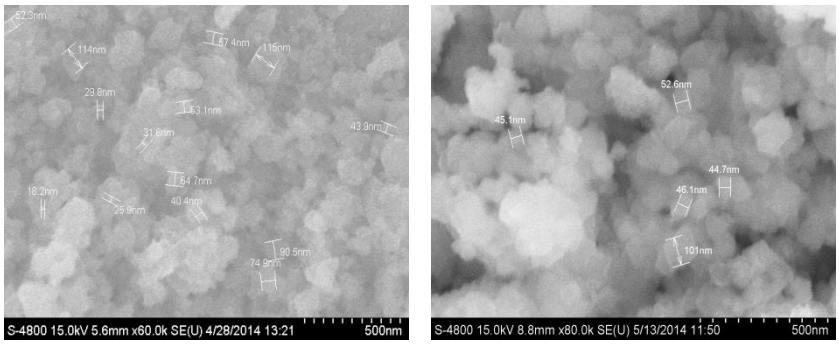

(c) 5 wt % SnO_2 doped MnO_2 (d) 7 wt % SnO_2 doped MnO_2

Fig. 3 Micrographs of SnO_2 doped MnO_2 samples

Fig. 3 depicts the SEM images of SnO_2 doped MnO_2 thick films. Fig. 3 (a) depicts the microstructure of SnO_2 (1 wt %) doped MnO_2 film consisting of smaller grains of SnO_2 are associated with the larger grains of MnO_2. The film consists of crystal like lumpsy structures spread over the grains of MnO_2 and voids having grain sizes ranging from 50 nm to 200 nm distributed non-uniformly. Fig. 3 (b) depicts the microstructure of SnO_2 (3 wt %) doped MnO_2 film, which consists large number of smaller grains of SnO_2 associated with the larger grains of MnO_2 as compared to that in Fig. 3 (a). The film consists of voids and a wide range of grains with grain sizes ranging from 10 nm to 200 nm distributed non-uniformly. Fig. 3 (c) depicts the microstructure of SnO_2 (5 wt %) doped MnO_2 film consisting of even smaller grains of SnO_2 in association with MnO_2 as compared to that in Figs. 3 (a and b). The most of the grains of MnO_2 are in contact with smaller grains of SnO_2. The films consist of voids and a wide range of variety of arranged grains with grain sizes ranging from 10 nm to 100 nm distributed non-uniformly. Fig. 3 (c) shows that the grains of MnO_2 and SnO_2 in the film are arranged one above the other to form compositions. This film was observed to be the sensitive to 200 ppm LPG at 350^oC. The MnO_2 - SnO_2 compositions in the film increases with doping concentration. Larger the doping concentration, larger would be the amount of SnO_2 contents in the bulk of the film, which changes the microstructure and hence the surface reactivity of the film and vice versa. The doping concentration was, therefore, optimized to have optimum number of SnO_2 grains in the bulk so as to contribute effective enhancement of LPG

sensing. Fig. 3 (d) depicts the microstructure of SnO_2 (7 wt %) doped MnO_2 film consisting of the SnO_2 grains are associated with the grains of MnO_2 forming the compositions of MnO_2 and SnO_2. Less response of this film to LPG may be attributed to the fact of formation of the compositions of MnO_2 and SnO_2 and agglomeration of all the grains which increases the entire grain size. Due to increase of the grain size, the effective surface to volume ratio decreases and hence the LPG response decreases. The further doping concentration (> 7 wt %) may again decrease the LPG response.

3.3 Electrical properties

3.3.1 I-V characteristics

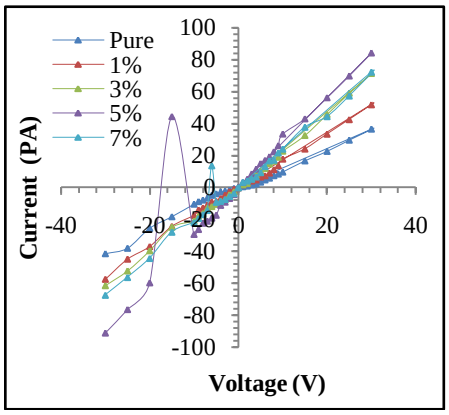

Fig. 4 I- V characteristics of (a) SnO_2 doped MnO_2 films

Figs. 4 depict I-V characteristics of pure, SnO_2 doped MnO_2 films. It is clear from the symmetrical nature of I-V characteristics that, the materials as well as silver contacts made on the films are ohmic in nature. The material is therefore said to have resistive properties.

3.3.2 Electrical conductivity

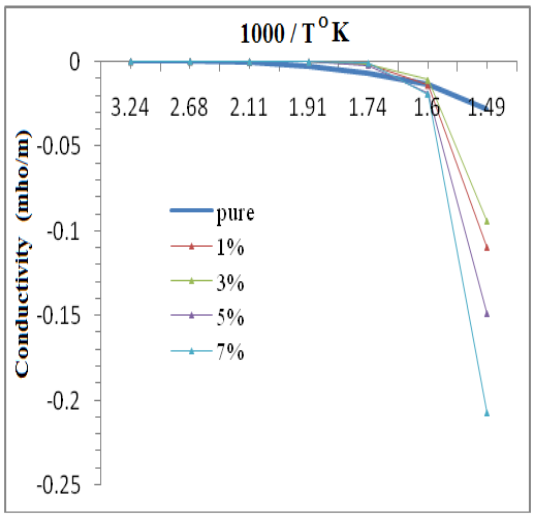

Fig. 5 Conductivity-temperature profile of SnO_2 doped MnO_2 films

Fig. 5 shows the variation of conductivity with the reciprocal of operating temperature of SnO_2 doped MnO_2 films. The conductivities of all samples are decreasing with increase in operating

temperature. The decrease in conductivity with increase in operating temperature could be attributed to positive temperature coefficient of resistance and the semiconducting nature of the SnO_2 modified MnO_2.

3.4 Gas sensing performance

3.4.1 Pure MnO_2 films

3.4.1.1 Effect of operating temperature

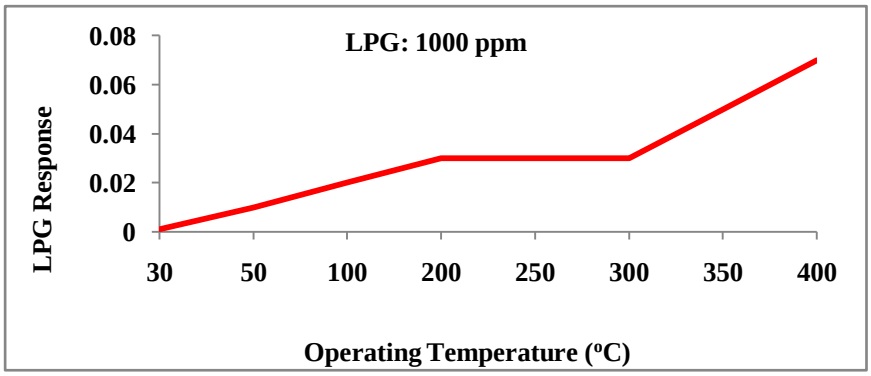

Fig. 6 Variation of LPG response of pure MnO_2 with operating temperature

Fig. 6 shows the variation of LPG (1000 ppm) gas response of pure MnO_2 thick films with operating temperature. It is observed from the Fig. 6 that, the LPG response is negligibly small from low temperature to 200°C and the response is steady from 200°C to 300°C. The LPG response increases with operating temperature beyond 300°C - 400°C, which is not desired. Maximum response obtained is of the order of 0.07 at 400°C, which is negligibly smaller. The monitoring of LPG at such a high temperature is most inconvenient. This is the main drawback of pure MnO_2 thick films as LPG sensors. So, it is the need to modify the bulk and / or surface of the base material to enhance the LPG sensing performance and its selective nature among the mixture of various gases, for large applicability.

3.4.1.2 Selectivity

It is observed from Fig. 7 that the pure MnO_2 is sensitive to H_2S at 400°C. The pure MnO_2 thick films are less sensitive to LPG among all the gases. This is the major drawback of pure MnO_2 thick films, while studying the LPG sensing profile of the sensor. So, it is the today's need to modify the pure MnO_2, to behave as the LPG sensor.

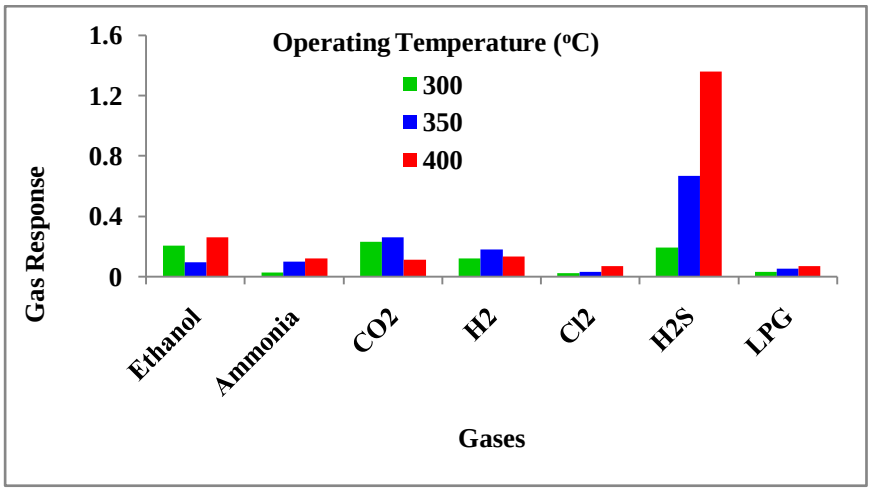

Fig. 7 Selectivity of pure MnO_2

3.4.2 SnO_2 doped MnO_2 Sensor

3.4.2.1 Effect of operating temperature

Fig. 8 depicts the variation of gas response of SnO_2 doped MnO_2 to LPG (200 ppm) with operating temperature. The maximum response of SnO_2 doped MnO_2 (5 wt %) to LPG was observed at 350^{0}C.

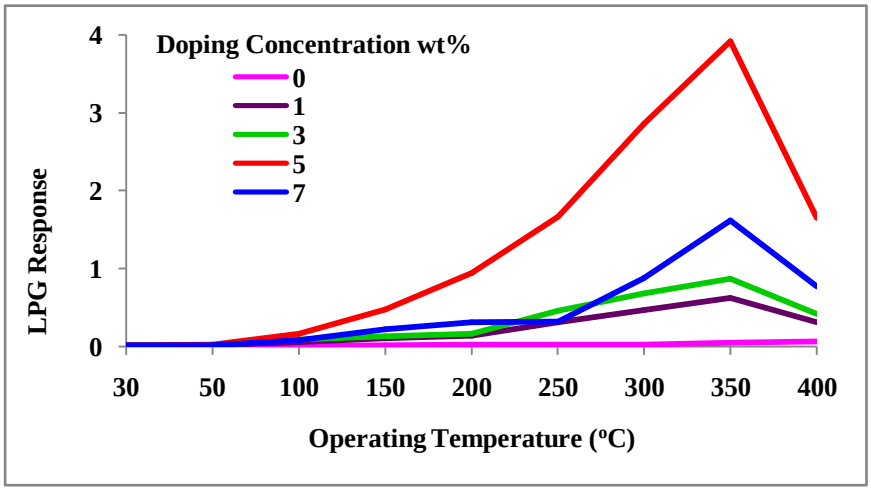

Fig. 8 Variation of LPG response with operating temperature

The response could be attributed to the adsorption-desorption type of mechanism of gas sensing. The quantity of oxygen physisorbed on the sensor surface would depend on the number of SnO_2 misfits on the MnO_2 surface and operating temperature. Response curve is sharp.

3.4.2.2 Active region of the sensor

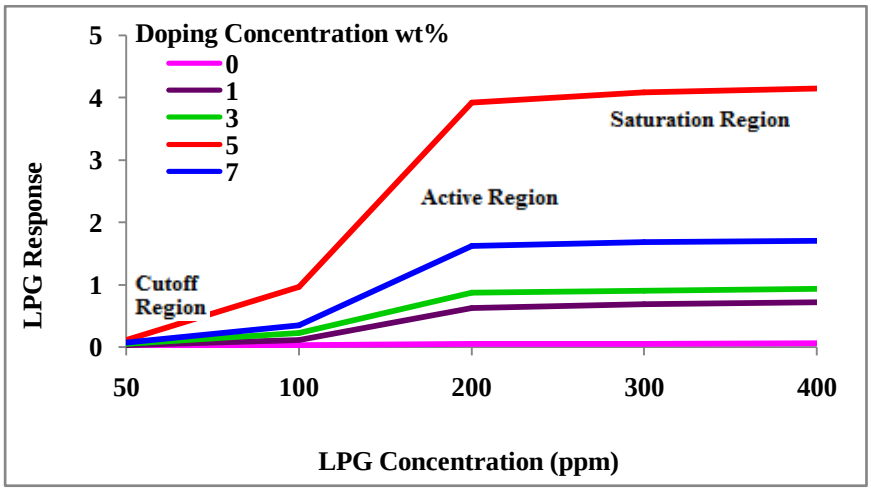

Fig. 9 Variation in LPG response with LPG concentration (ppm)

The variation of gas responses of SnO_2 doped MnO_2 samples with LPG gas concentration are represented in Fig. 9. It is clear from the figure that the gas responses go on increasing linearly with gas concentration up to 200 ppm. The rate of increase in response was relatively larger up to 200 ppm and saturated beyond 200 ppm. The monolayer of the gas molecules formed on the surface could cover the whole surface of the film. The gas molecules from that layer would reach the surface active sites of the film. Thus, the active region of the sensor would be up to 200 ppm. For proper functioning of the sensor, one should work in the active region only.

3.4.2.3 Effect of doping concentration

It is clear from the observations that, the change in doping concentration in wt % of SnO_2 into MnO_2 changes the sensing habits and therefore it may sense different gases at different level of doping. Fig. 10 indicates the LPG response as a function of the amount of doping (wt %) of SnO_2 in MnO_2. SnO_2 (5 wt %) doped MnO_2 sample was observed to be the sensitive to LPG at 350^{0}C. The higher response to LPG (200 ppm) may be attributed to the optimum porosity and largest effective surface area available to react the gas molecules and appropriate number of SnO_2 misfits to adsorb the oxygen which in turn would oxidize the exposed gas.

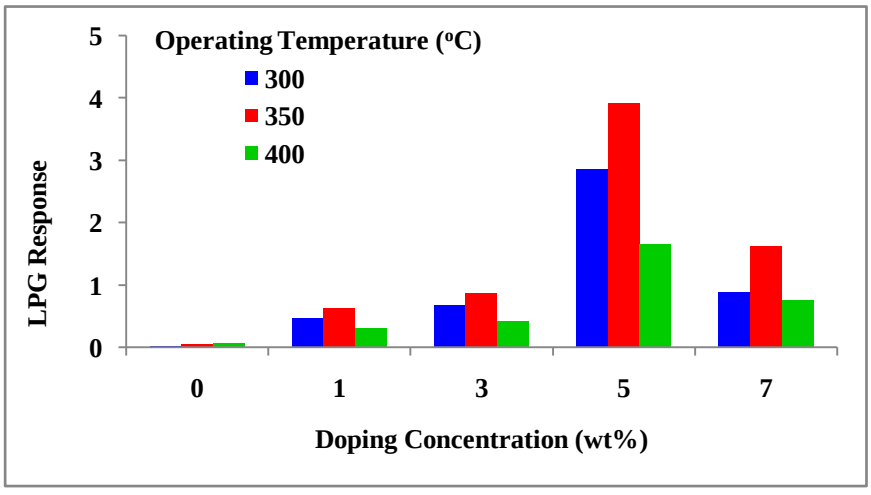

Fig. 10 Variation of LPG response with wt % of SnO_2 in MnO_2 samples

3.4.2.4 Selectivity

It is observed from Fig. 11 that the SnO_2 doped (5 wt %) MnO_2 sensor gives maximum response to LPG (200 ppm) at 350^{0}C. The sensors showed the high selectivity for LPG, NH_3 and H_2S among all other tested gases viz. CO_2, ethanol, H_2 and Cl_2. The sensor responds to LPG, NH_3 and H_2S at 350^{0}C. i. e. It has less selectivity to LPG in comparison with NH_3 and H_2S. This is the major drawback of this sensor.

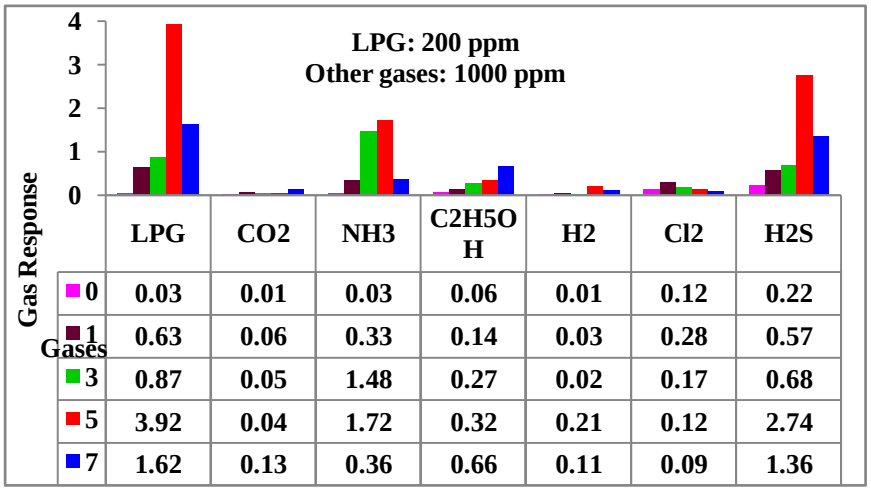

Gases	LPG	CO2	NH3	C2H5OH	H2	Cl2	H2S
0	0.03	0.01	0.03	0.06	0.01	0.12	0.22
1	0.63	0.06	0.33	0.14	0.03	0.28	0.57
3	0.87	0.05	1.48	0.27	0.02	0.17	0.68
5	3.92	0.04	1.72	0.32	0.21	0.12	2.74
7	1.62	0.13	0.36	0.66	0.11	0.09	1.36

Fig. 11 Selectivity of LPG from mixture of gases

3.4.2.5 Response and Recovery Time

The response and recovery of the SnO_2 doped MnO_2 (5 wt %) sensor is represented in Fig. 12. The response and recovery of the sensor was quick (~ 30 s) to 200 ppm of LPG. The quick response may be due to faster oxidation of gases.

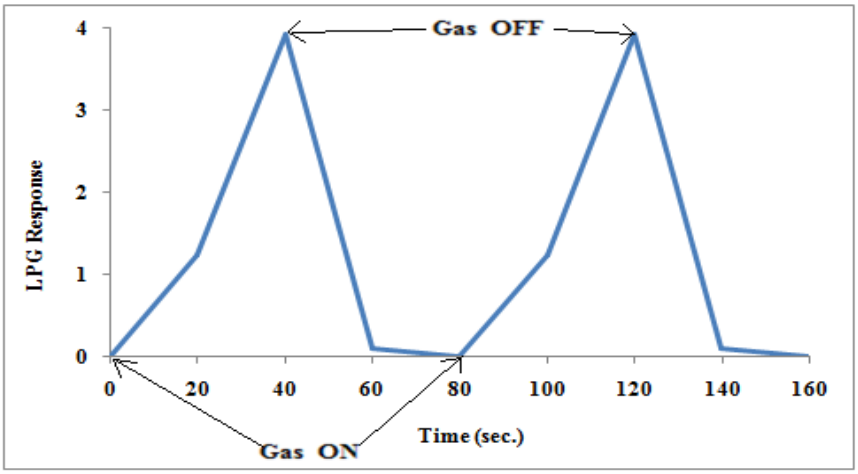

Fig. 12 Response and recovery of SnO_2 doped MnO_2 sample

For better performance of the sensor, the recovery should be fast.

Summary Table

Samples	Gas sensing performance					Optimum operating conditions	
	Gas under study	Gas response	Gas conc. (ppm)	Response time (s)	Recovery time (s)	Op. temp. (^{0}C)	Dop. Conc. (wt. %)
Pure MnO_2	LPG	0.07	1000	60	60	400	-----
SnO_2 doped MnO_2	LPG	3.92	200	30	30	350	5

3.5 Discussion: LPG gas sensing mechanism

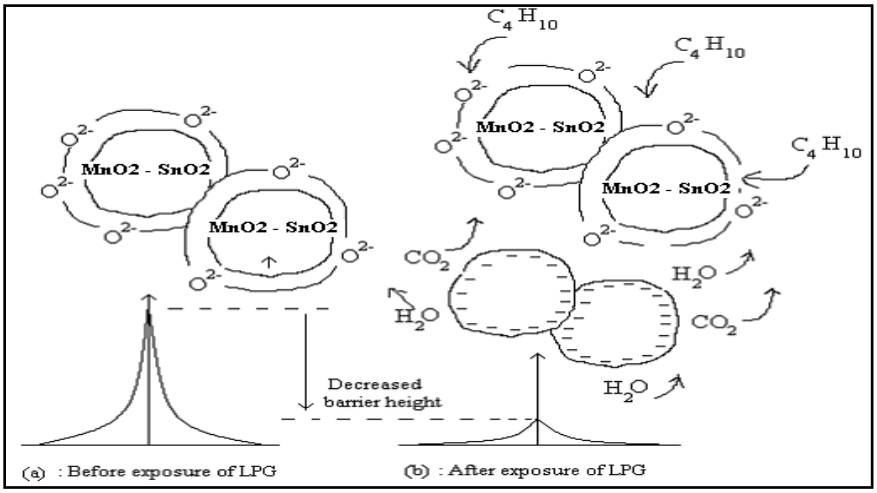

Fig. 13 LPG gas sensing mechanism of SnO_2 activated MnO_2 films at 350^{0}C

As the butane is the major constituent of LPG, it requires high temperature to dissociate into lower weight alkanes. C-C and C-H bonds are quite strong due to strong Vander Waals forces. They break only at higher temperatures resulting in carbon and hydrogen separation. The atmospheric oxygen O_2 adsorbs on the surface of the thick film. It captures the electrons from conduction band as:

$$O_{2\,(air)} + 4e^- \rightarrow 2O^{2-}{}_{(film\ surface)}$$

It results in decrease in the conductivity of the film.

When alkanes made reaction with oxygen, complex reactions take place, ultimately converting the alkanes to carbon dioxide and water as:

$$CH_{4\,(gas)} + 4\,O^{2-}{}_{(film\ surface)} \rightarrow CO_{2\,(gas)} + 2\,H_2O_{\,(gas)} + 8\,e^-{}_{(cond.\ band)}$$

$C_2H_{6\,(gas)} + 7\ O^{2-}{}_{(film\ surface)} \rightarrow 2\ CO_{2\,(gas)} + 3\ H_2O_{(gas)} + 14\ e^-{}_{(cond.\ band)}$

$C_3H_{8\,(gas)} + 10\ O^{2-}{}_{(film\ surface)} \rightarrow 3\ CO_{2\,(gas)} + 4\ H_2O_{(gas)} + 20\ e^-{}_{(cond.\ band)}$

$C_4H_{10\,(gas)} + 13\ O^{2-}{}_{(film\ surface)} \rightarrow 4\ CO_{2\,(gas)} + 5\ H_2O_{(gas)} + 26\ e^-{}_{(cond.\ band)}$

This shows n-type conduction. Molecular oxygen O_2 becomes O_2^- at high temperature and alkanes decompose producing hydrogen ions H^+ in the reaction. The anion super-oxide O_2^- reacts with H^+ giving water molecule and molecular oxygen O_2:

$$2O_2^- + 2\ H^+ \rightarrow H_2O_2 + O_2$$

$$2\ H_2O_2 \rightarrow 2\ H_2O + O_2$$

LPG gas on exposure decomposes into carbon and hydrogen species which react with adsorbed oxygen, liberating the captured electrons into conduction band resulting in enhancing the catalytic activity of the film surface.

3.6 Summary

From the results obtained, following conclusions can be made for the LPG sensing performance of the sensors.

1. Pure manganese oxide was almost insensitive to LPG traces.
2. SnO_2 as the additive in MnO_2 is outstanding in promoting the LPG sensing.
3. 5 wt% SnO_2 doped MnO_2 was found to be sensitive to LPG at 350^0C, but has less selectivity.
4. SnO_2 modified MnO_2 has the potential of fabricating the LPG sensor.
5. The sensor showed very rapid response and recovery to LPG.
6. The sensor has good selectivity to LPG against Ammonia, Ethanol, CO_2, Cl_2, H_2 and H_2S at 350^0C.

References:

1. Adachi M., Okuyama K., Kousaka Y. and Tanaka H. (1988) J. Aerosol Sci. 19(2): 253 – 263.
2. Seiyama T., Kato A., Fujiishi K. and Nagatani M. (1962) Anal. Chem. 34, 1502 – 1503.
3. McAleer J.F., Moseley P.T., Noris J.O.W, Williams D.E and Tofield B.C. (1987) J. of Chem. Soc., Faraday Transactions 1 83, 1323 – 1346.
4. G¨opel W., ed.: Sberveglieri G. (1992) Kluwer Academic Publishers 365 – 409.
5. Martinelli G., Carotta M.C., Traversa E. and Ghiotti G. (1999) MRS Bulletin, 30 – 36.
6. Ihokura K., Tanaka K. and Murakami N. (1983) Sens. Actuators 4, 607 – 612.
7. Wada K. and Egashira M. (2000) Sens. Actuators B 62, 211 – 219.
8. Shimizu Y. and Egashira M. (1999) MRS Bulletin 24, 18 – 24.
9. Zampiceni E., Bontempi E., Sberveglieri G. and Depero L.E. (2002) Thin Solid films 418, 16 – 20.
10. Dieguez A., Romano-Rodriguez A., Morante J.R., Kappler J., Barsan N. and G¨opel W. (1999) Sens. Actuators B 60, 125 – 137.
11. Yoo K.S., Cho N.M., Song H.S. and Jung H.J. (1995) Sens. Actuators B 25, 474 – 477.
12. Pan X.Q., Fu L. (2001) J. Appl. Phys. 89, 6048 – 6055.
13. Sakai G., Baik N.S., Miura N. and Yamazoe N. (2001) Sensors and Actuators B77, 116 – 121
14. Dutaive M S, Lalauze R and Pijolat C Sens. Actuators B 26 (1995) 27 38
15. Coutts T J, Pearsall N M and Tarricane L ; J. Vac. Sci. Technol. B2 (1984) 140
16. Coutts T J, Li X and Cessert T A; IEEE Electron Lett. 26 (1990) 660
17. Gardener J W, Shurmer H V and Corcoran P, Sens. Actuators B 4 (1991) 117

18. Lalweze R and Pizolat C; Sens. Actuators B 5 (1984)55
19. Tarey R D and Raju T A; Thin Solid Films 221 (1985) 181
20. Lane D W, Coath J A and Beldon H S; Thin Solid Films 221 (1992) 262
21. Karasawa T and Miyata Y Thin Solid Films 223 (1993) 135
22. Kulkarni A K and Knickerbocker S A Thin Solid Films 220 (1992) 321
23. Park S S, Zheng H and Mackenzie J D Thin Solid Films 258 (1995) 268